ISSN 1027-4510, Journal of Surface Investigation: X-ray, Synchrotron and Neutron Techniques, 2020, Vol. 14, No. 1, pp. 47–53. © Pleiades Publishing, Ltd., 2020.
Russian Text © The Author(s), 2020, published in Poverkhnost', 2020, No. 1, pp. 60–67.

$CoPt–Al_2O_3$ Nanocomposite Films: Synthesis, Structure, and Magnetic Properties

V. S. Zhigalov[a, *], L. E. Bykova[a, **], V. G. Myagkov[a], A. N. Pavlova[b], M. N. Volochaev[a], A. A. Matsynin[a], and G. S. Patrin[a, c]

[a] *Kirensky Institute of Physics, Krasnoyarsk Scientific Center, Siberian Branch, Russian Academy of Sciences, Krasnoyarsk, 660036 Russia*

[b] *Siberian State University of Science and Technology, Krasnoyarsk, 660014 Russia*

[c] *Siberian Federal University, Krasnoyarsk, 660041 Russia*

**e-mail: zhigalov@iph.krasn.ru*

***e-mail: lebyk@iph.krasn.ru*

Received January 14, 2019; revised February 18, 2019; accepted February 21, 2019

Abstract—The structure and magnetic properties of $CoPt–Al_2O_3$ nanocomposite films synthesized by the annealing of $Al/(Co_3O_4 + Pt)$ bilayers on a MgO(001) substrate at 650°C in vacuum are investigated. The synthesized composite films contain ferromagnetic CoPt grains with an average size of 25–45 nm enclosed in a nonconducting Al_2O_3 matrix. The saturation magnetization ($M_s \sim 330$ G) and coercivity ($H_c \approx 6$ kOe) of the films are measured in the film plane and perpendicular to it. The obtained films are characterized by a spatial rotational magnetic anisotropy, which makes it possible to arbitrarily set the easy magnetization axis in the film plane or perpendicular to it using a magnetic field stronger than the coercivity ($H > H_c$).

Keywords: thin films, ferromagnetic nanocomposites, CoPt alloy, magnetic anisotropy

DOI: 10.1134/S102745102001022X

INTRODUCTION

In recent years, composite nanomaterials have been the object of numerous studies due to their novel functional properties that differ from the properties of their constituents [1]. Composite ferromagnetic films containing transition-metal (Co, Fe, or Ni) nanoclusters in a dielectric or semiconductor matrix obtained by different physical and chemical methods have been intensively investigated [2–16]. Previously, $Fe–In_2O_3$ [12], $Co–In_2O_3$ [13], $Co–Al_2O_3$ [14, 15], $Fe–ZrO_2$ [16], and $Co–ZrO_2$ [17] ferromagnetic nanocomposite films were synthesized using thermite reactions.

FePd, FePt, and CoPt thin films with $L1_0$-type ordering are characterized by a high magnetic-anisotropy constant K_1 ($K_1 > 3 \times 10^7$ erg/cm^3) and an easy magnetization axis perpendicular to the film surface (so-called perpendicular magnetic anisotropy). Nanocomposite films containing isolated high-coercivity $L1_0$ clusters in a nonmagnetic matrix [18–25] can be used in high-density magnetic data storage.

To date, there have been a great number of studies on the synthesis and investigation of nanocomposites containing $L1_0$-CoPt and $L1_0$-FePt nanoparticles in oxide matrices [18, 19, 22–25]. These investigations are important for application in the synthesis of nanocomposites with the desired magnetic, structural, and transport properties.

In this work, we report on the results of the synthesis and investigations of the structure and magnetic properties of high-coercivity $CoPt–Al_2O_3$ nanocomposite films. The films are synthesized by the solid-state reaction in the $Al/(Co_3O_4 + Pt)/MgO$ film system with annealing in vacuum at a temperature of 650°C for 1 h. The main synthesis parameters, including the initiation temperature and phase composition of the reagents and reaction products, are determined. The synthesized samples exhibited spatial rotational magnetic anisotropy, which makes it possible to set the easy magnetization axis in any spatial direction (in the film plane or perpendicular to it) in a magnetic field stronger than the coercivity, which is retained after switching-off the external magnetic field. High-coercivity nanocomposite films with rotational magnetic anisotropy can be used in devices with a tunable easy axis.

EXPERIMENTAL

Figure 1 shows the scheme of synthesizing $CoPt–Al_2O_3$ nanocomposite films. First, we prepared the high-coercivity $L1_0$-CoPt(111) ferromagnetic films using the technique described in [26], which included

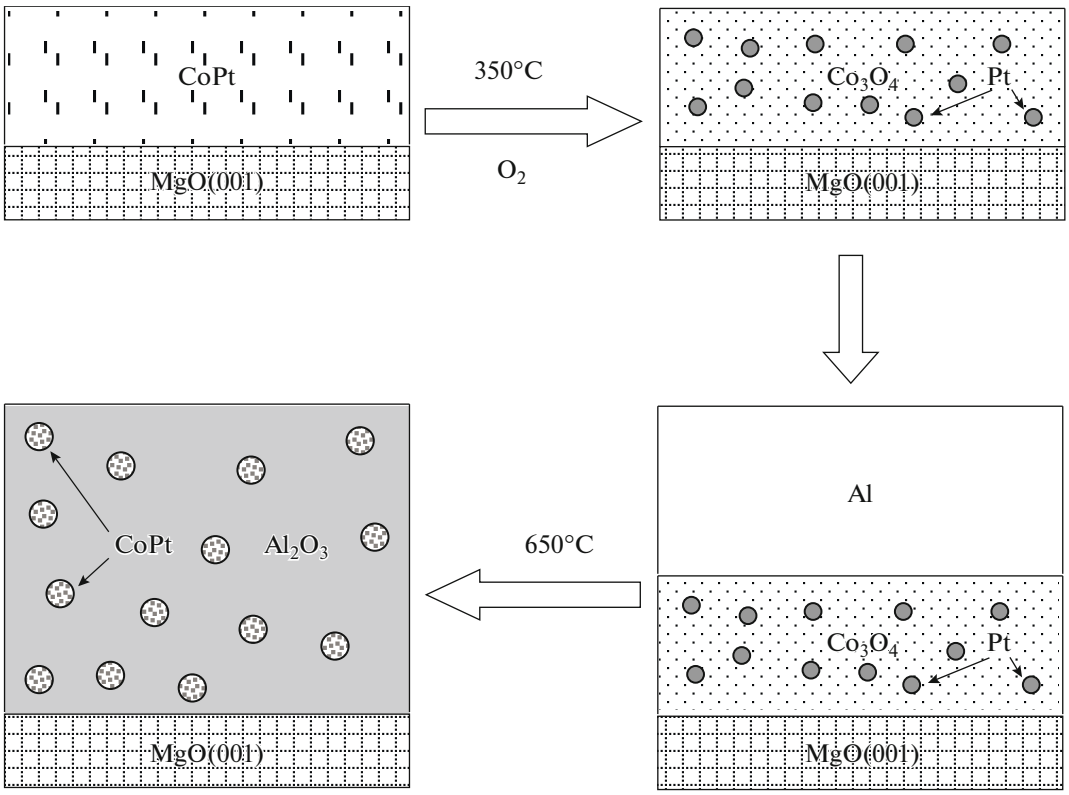

Fig. 1. Schematic of the formation of the CoPt–Al_2O_3 nanocomposite films.

the magnetron sputtering of Pt films with a thickness of ~50 nm in vacuum at a residual pressure of 10^{-6} Torr onto a MgO(001) substrate heated to a temperature of 250°C, which ensured epitaxial growth of the Pt(111) plane relative to the substrate surface, the thermal deposition of a polycrystalline Co film with a thickness of ~70 nm in vacuum at a residual pressure of 10^{-6} Torr onto a Pt film at room temperature to prevent a reaction between the layers (the chosen thicknesses of the reacting layers were ~70 nm for Co and ~50 nm for Pt, which provided an equiatomic composition), and annealing of the obtained Co/Pt(111)/MgO bilayer samples in vacuum at 10^{-6} Torr at a temperature of 650°C for 90 min. After annealing of the Co/Pt(111)/MgO samples, the magnetically hard $L1_0$-CoPt(111) phase forms in the Co/Pt(111) film structure based on the oriented Pt(111) layer [26].

Then, the $L1_0$-CoPt/MgO films were oxidized in air at a temperature of ~550°C for 3 h. The oxidation yielded a Co_3O_4 + Pt film structure containing Pt nanoclusters dispersed in a Co_3O_4 matrix. It should be noted that, in the method used, Co was oxidized, while Pt remained unoxidized.

At the next stage, an Al layer with a thickness of ~140 nm was thermally deposited onto the Co_3O_4 + Pt film surface in vacuum at a pressure of 10^{-6} Torr. To prevent an uncontrolled reaction between the layers, Al was deposited at room temperature. This yielded the initial Al/(Co_3O_4 + Pt)/MgO(001) film structure.

The CoPt–Al_2O_3 nanocomposite films were obtained by annealing of the initial Al/(Co_3O_4 + Pt)/MgO(001) samples in vacuum at 10^{-6} Torr in the temperature range of 350–650°C with a step of 50°C and exposure at each temperature for 40 min. After each annealing, the film magnetization was measured. The formation of the Co and CoPt magnetic phases was detected by the occurrence of magnetization. In these measurements, the temperatures of the initiation and end of CoPt–Al_2O_3 nanocomposite synthesis were determined

The thicknesses of the reacting layers were determined by X-ray fluorescence analysis. The saturation magnetization M_s and coercivity H_c were measured on a vibrating sample magnetometer in magnetic fields of up to 20 kOe. The torque curves were measured with a torque magnetometer in a maximum magnetic field of 17 kOe. The phase composition was investigated by X-ray diffraction using a DRON-4-07 diffractometer in CuK_α radiation ($\lambda = 0.15418$ nm). The structure of the synthesized films was examined by transmission electron microscopy on a Hitachi HT7700 microscope equipped with a Bruker X-Flash 6T/60 energy dispersive spectrometer at an accelerating voltage of 100 kV. Cross sections were prepared using a Hitachi FB2100 focused-ion-beam (FIB) system. The tem-

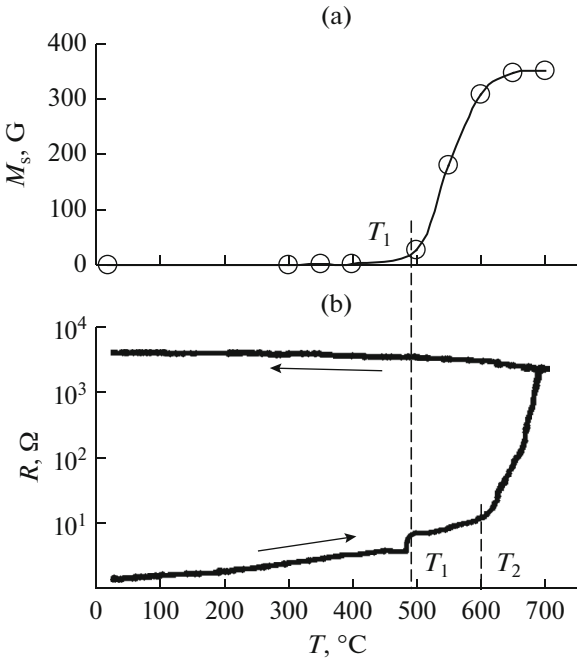

Fig. 2. Dependence of (a) the saturation magnetization M_s and (b) electrical resistance R on the temperature T of annealing the Al/(Co_3O_4 + Pt)/MgO film.

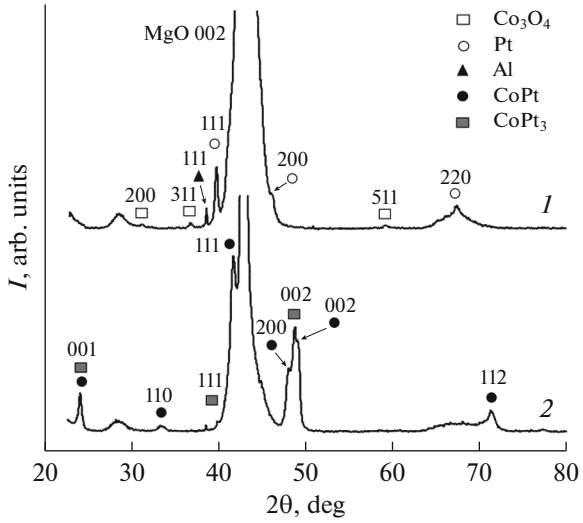

Fig. 3. X-ray diffraction patterns of the Al/(Co_3O_4 + Pt)/MgO film (*1*) before and (*2*) after annealing at 650°C.

perature dependence of the electrical resistance of the Al/(Co_3O_4 + Pt) film was measured by the four-probe method using pressed contacts in vacuum at 10^{-6} Torr at a heating rate of ~5 deg/min.

RESULTS AND DISCUSSION

Cobalt reduction and the formation of CoPt ferromagnetic grains were investigated by measuring the saturation magnetization of the initial Al/(Co_3O_4 + Pt)/MgO(001) samples as a function of the annealing temperature ($M_s(T)$) (Fig. 2a). It can be seen from the $M_s(T)$ dependence that, below ~490°C, Co reduction processes do not occur in the investigated Al/(Co_3O_4 + Pt) structure and its magnetization is therefore close to zero. The magnetization sharply increases at $T >$ 500°C. Annealing at $T >$ 650°C facilitates the occurrence of the maximum number of CoPt grains.

Figure 2b shows the temperature dependence of the electrical resistance of the Al/(Co_3O_4 + Pt)/MgO(001) film. It can be seen that, below ~490°C, the resistance is of the metallic type, which is determined by the upper aluminum layer, and the layers do not intermix. The $R(T)$ dependence includes two portions: near T_1 ~ 490°C and near T_2 ~ 600°C. It is well-known [14] that T_1 is close to the temperature ~500°C of Co reduction of the Co_3O_4 oxide in the Al/Co_3O_4 film system. At the same time, it is well-known [27] that the $L1_0$-CoPt phase starts forming at a temperature of ~375°C in the Pt/Co films. We can conclude that, at T_1 ~ 490°C, the reaction of Co reduction from the Co_3O_4 oxide with the formation of the CoPt and Al_2O_3 phases begins. As was shown in [27], the $CoPt_3$ phase forms at a temperature of ~575°C, which is similar to T_2 ~ 600°C. As a result, at temperatures above 600°C, the electrical resistance of the film sharply grows, which indicates continuation of the solid-state reaction in the Al/(Co_3O_4 + Pt)/ MgO(001) film with the formation of CoPt, $CoPt_3$, and Al_2O_3 phases.

The temperature of initiation of the reaction $T_{in} = T_1 \approx$ 490°C in the Al/(Co_3O_4 + Pt)/MgO(001)-film system determined from the $R(T)$ dependence coincides with the temperature T_1 in the annealing temperature dependence of the magnetization ($M_s(T)$). In addition, these dependences were used to determine the temperature of the end of the reaction and the formation of CoPt grains (~650°C).

X-ray measurements performed after the formation of the CoPt(111) film and deposition of the Al layer showed that the obtained system consists of Co_3O_4, Pt, and Al (curve *1* in Fig. 3). Annealing at a temperature of 650°C led to the formation of the ordered $L1_0$–CoPt tetragonal phase in the reaction products, which is confirmed by the presence of the 001 superstructural reflection and the ordered $CoPt_3$ cubic phase (the 001 superstructural reflection) (curve *2* in Fig. 3). Reflections of the Al_2O_3 phase were not observed because of its high dispersion.

The structure of the synthesized films was investigated also by transmission electron microscopy. The electron diffraction pattern of the obtained CoPt–Al_2O_3 samples (Fig. 4, Table 1) contains reflections of the ordered $L1_0$–CoPt and $L1_2$–$CoPt_3$ phases (this is indicated by the superstructural and fundamental 001 and 002 reflections of the $L1_0$–CoPt phase and the

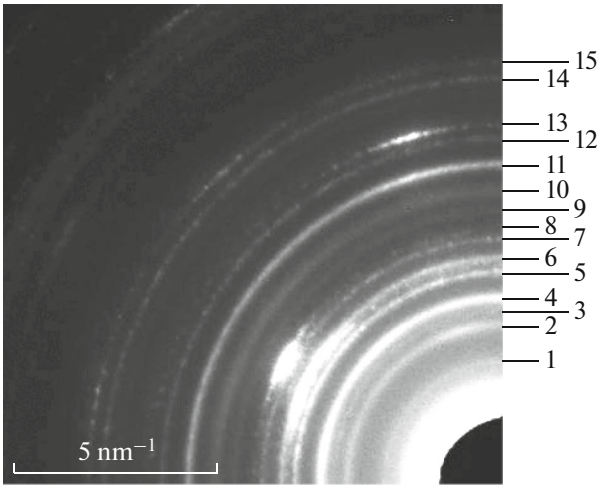

Fig. 4. Electron diffraction pattern of the CoPt–Al_2O_3 nanocomposite film.

100 and 200 reflections of the $L1_2$–$CoPt_3$ phase) and the α-Al_2O_3 and γ-Al_2O_3 phases, as well as a small amount of aluminum spinel $CoAl_2O_4$.

The cross sections of the Al/(Co_3O_4 + Pt)/MgO(001) film (Fig. 5a) before and after annealing at T = 650°C (Fig. 5b) show that it consists of Co_3O_4 + Pt and Al layers and, after annealing, the CoPt–Al_2O_3 composite forms. This is confirmed by X-ray and electron microscopy measurements.

The electron microscopy image of the synthesized CoPt–Al_2O_3 sample surface (Fig. 6) shows that CoPt nanoparticles are uniformly distributed over the reaction product. The mean atomic number of the Al_2O_3 phase sample is smaller than that of CoPt and therefore the dark areas correspond to CoPt grains and the bright areas, to Al_2O_3. The average CoPt grain size is between 25–45 nm.

Table 1. Identification of the *hkl* diffraction reflections in the CoPt–Al_2O_3 nanocomposite film

Ring number	CoPt	$CoPt_3$	α-Al_2O_3	γ-Al_2O_3	$CoAl_2O_4$
1	001	100	–	–	–
2	–	–	–	–	220
3	–	110	–	220	–
4	110	–	104	–	–
5	–	111	–	222	–
6	111	–	113	–	–
7	–	200	–	–	400
8	002	–	–	400	331
9	–	210	024	–	–
10	201	–	116	–	422
11	112	211	018	511	511
12	–	220	214	400	440
13	220	–	–	–	–
14	–	310	–	–	–
15	311	–	–	–	–

X-ray diffraction and electron microscopy data allow us to conclude that the film after annealing contains CoPt ($L1_0$-CoPt + $L1_2$-$CoPt_3$) nanograins surrounded by Al_2O_3. The synthesis of the nanocomposite includes the three successive solid-state reactions

$$\sim 490^\circ C \rightarrow 8Al + 3Co_3O_4 \rightarrow 9Co + 4Al_2O_3, \quad (1)$$

$$\sim 490^\circ C \rightarrow Co + Pt \rightarrow L1_0\text{-}CoPt, \quad (2)$$

$$\sim 600^\circ C \rightarrow L1_0\text{-}CoPt + 2Pt \rightarrow L1_2\text{-}CoPt_3. \quad (3)$$

In the synthesized samples, we observed spatial rotational magnetic anisotropy with the easy axis that can be rotated in fields exceeding the coercivity both in the sample plane and perpendicular to it, which was demonstrated by the torque-magnetometer investigations (Figs. 7 and 8).

Figure 7 shows a schematic of the easy-axis (EA) rotation and the torque curve $L_{\|}(\varphi)$ in the plane of the synthesized CoPt–Al_2O_3 film (the forward (φ = 0°–360°) and reverse (360°–0°) paths) in a magnetic field of 10 kOe. The experiments showed that the EA was aligned from the initial position EA_0 to the direction EA_φ in the film plane upon rotation of the magnetic field H by angle φ in the sample plane and retained this direction after switching-off the external magnetic field. The torque curve exhibited rotational hysteresis (retardation by angle α). To quantitatively characterize the magnetic rotational anisotropy, in [26] we introduce the constant $L_{\|}^{rot}$, which was defined as a shift of the torque curve upon rotation of the magnetic field clockwise ($+L_{\|}^{rot}$) and counterclockwise ($-L_{\|}^{rot}$), i. e., ($L_{\|}^{rot} = +L_{\|}^{rot} = -L_{\|}^{rot}$ (Fig. 7). It can be seen from the curve that a rotational magnetic anisotropy with a value of $L_{\|}^{rot} \approx 7 \times 10^5$ erg/cm^3 is induced in the film and there is a small contribution of the uniaxial anisotropy $K_0 \sin 2\varphi$, where $K_0 \approx 1.5 \times 10^5$ erg/cm^3 is the uniaxial anisotropy constant.

Figure 8 shows a schematic of the EA rotation and the torque curve $L_{\perp}(\varphi)$ perpendicular to the CoPt–Al_2O_3 film plane (the forward (0°–360°) and reverse (360°–0°) paths) in a magnetic field of 10 kOe. The easy axis was aligned from its initial position EA_0 to the direction EA_φ perpendicular to the film plane upon rotation of the magnetic field H by angle φ perpendicular to the sample plane with regard to retardation by angle α and retained this direction after switching-off the external magnetic field. Upon rotation of the magnetic field perpendicular to the sample plane (Fig. 8), the torque can be decomposed into rotational mag-

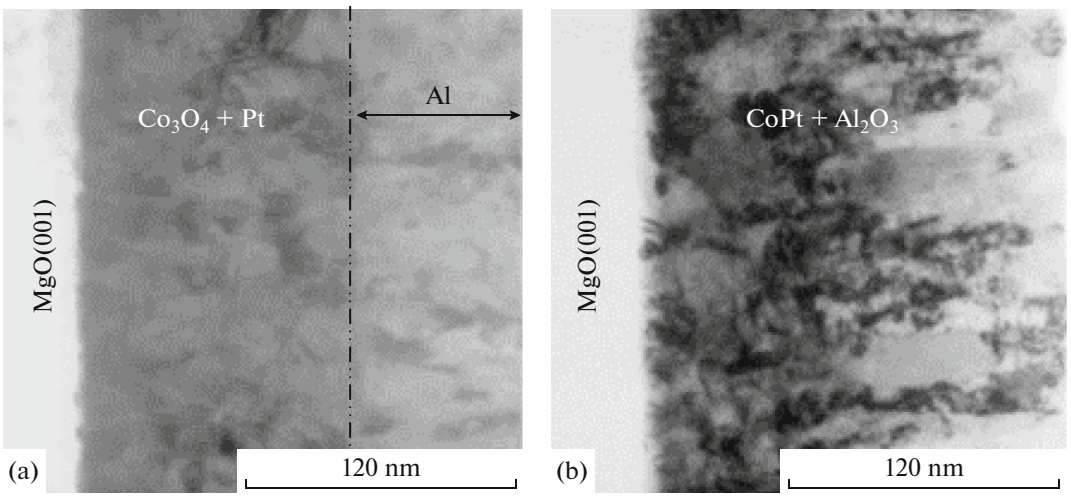

Fig. 5. Cross-sectional image of the Al/(Co_3O_4 + Pt)/MgO film (a) before and (b) after annealing at $T = 650$°C.

netic anisotropy $L_{\perp}^{rot} \approx 7 \times 10^5$ erg/cm^3 and uniaxial anisotropy with $K_0 \approx 2.5 \times 10^5$ erg/cm^3.

In the presence of rotational magnetic anisotropy in the films, the hysteresis loops are identical in all spatial directions [27, 28]. Figure 9 presents the hysteresis loops measured in the CoPt–Al_2O_3 film plane and perpendicular to it. They have similar shapes, a coercivity of $H_c \approx 6$ kOe, and a saturation magnetization of $M_s \sim 330$ G in both directions. The study of the CoPt–AlN [22], CoPt–TiO_2, and FePt–TiO_2 [24] nanocomposite films showed that they have identical hysteresis loops in the film plane and perpendicular to it. Therefore, we can assume that these films, similar to the samples investigated here, are characterized by rotational magnetic anisotropy. The sources of this anisotropy suggested in publications include domain-structure rearrangement, martensitic transformations, and controlled magnetostriction. However, there is still a lack of convincing models that would explain this effect. Previously, we studied the formation of rotational magnetic anisotropy in polycrystalline δ-$Mn_{0.6}Ga_{0.4}$ [28], MnBi [29], and $Co_{28}Pt_{72}$ [27] and epitaxial $L1_0$-CoPt(111) [26] thin films. In [26], a possible mechanism responsible for the occurrence of the anisotropy was considered to be the magnetic exchange interaction between the $L1_0$-CoPt and $L1_2$-$CoPt_3$ phases. The formation of these phases is observed in the investigated CoPt–Al_2O_3 nanocomposite films. Rotational magnetic anisotropy in the synthesized

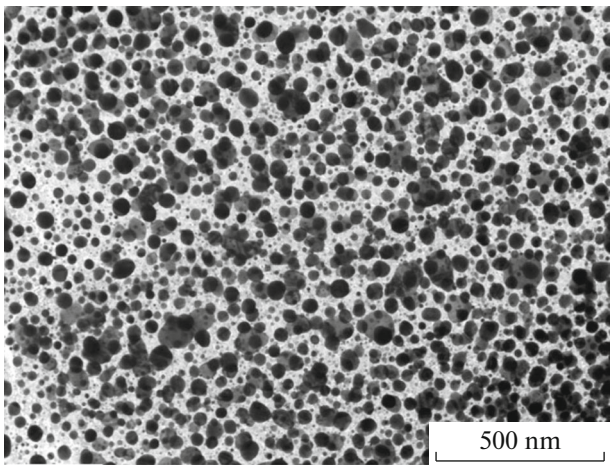

Fig. 6. Electron microscopy image of the CoPt–Al_2O_3 nanocomposite film surface. Dark areas correspond to CoPt grains and light areas, to the Al_2O_3 matrix.

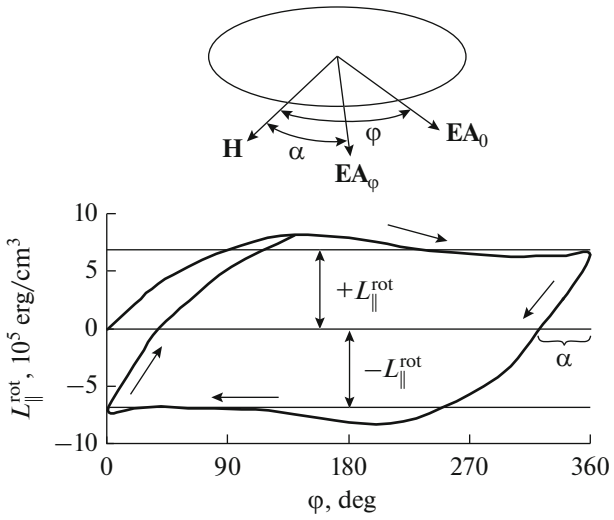

Fig. 7. Schematic of rotation of the easy axis (EA) and torque curve $L_{\parallel}^{rot}(\varphi)$ in the CoPt–Al_2O_3 film plane (the forward (φ = 0°–360°) and reverse (360°–0°) paths) in a magnetic field of 10 kOe.

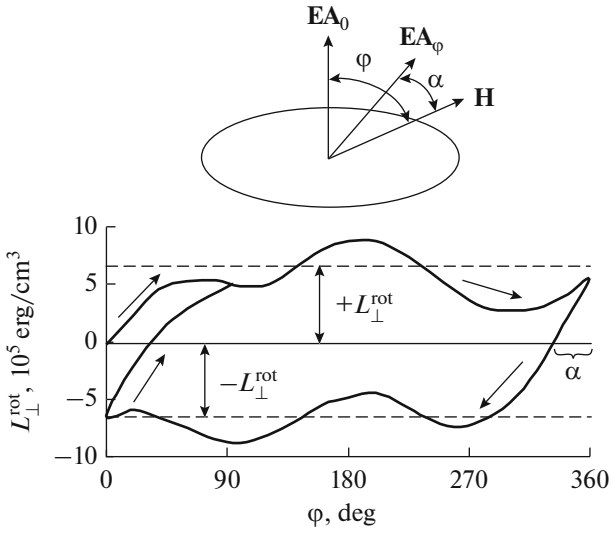

Fig. 8. Schematic of rotation of the easy axis (EA) and torque curve $L_\perp^{rot}(\varphi)$ perpendicular to the CoPt–Al_2O_3 film plane (the forward ($\varphi = 0°–360°$) and reverse ($360°–0°$) paths) in a magnetic field of 10 kOe.

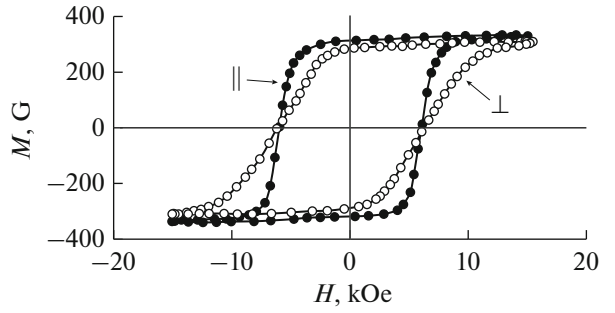

Fig. 9. Hysteresis loops in the CoPt–Al_2O_3 nanocomposite film plane and perpendicular to it.

films can be explained by the exchange magnetic interaction between the $L1_0$-CoPt and $L1_2$-$CoPt_3$ phases contained in CoPt grains.

CONCLUSIONS

Thus, the main results of the investigations are as follows. The high-coercivity CoPt–Al_2O_3 nanocomposite films were synthesized by annealing of the Al/(Co_3O_4 + Pt)/MgO film system in vacuum at a temperature of 650°C for 1 h. The synthesis-initiation temperature was found to be ~490°C. Comprehensive structural and magnetic investigations unambiguously indicate the formation of CoPt ($L1_0$-CoPt + $L1_2$-$CoPt_3$) ferromagnetic clusters with an average size of 25–45 nm in a nonconducting Al_2O_3 matrix in the reaction products; the saturation magnetization was found to be ~330 G/cm^3 and the coercivity was ~6 kOe. The synthesized samples are characterized by spatial rotational magnetic anisotropy with the easy axis that can be set in the sample plane or perpendicular to it by a magnetic field exceeding the coercivity and the direction can be retained after switching-off the magnetic field. The rotational magnetic anisotropy in the obtained films is explained by the exchange magnetic interaction between the phases $L1_0$-CoPt and $L1_2$-$CoPt_3$ contained in CoPt grains. Study of the mechanisms and conditions for the occurrence of rotational magnetic anisotropy in the films can be used to create nanoscale devices with a tunable easy magnetization axis. Thus, the solid-state method is promising for the synthesis of nanocomposite thin films with ferromagnetic clusters enclosed in oxide matrices with high magnetization and chemical stability.

ACKNOWLEDGMENTS

We thank D.A. Velikanov for measuring the hysteresis loops of the samples and G.N. Bondarenko for carrying out the X-ray structural experiments. Electron microscopy investigations of the sample surface and cross section were carried out using equipment of the Center of Collective Use of the Krasnoyarsk Scientific Center, Siberian Branch, Russian Academy of Sciences.

FUNDING

This study was supported by the Russian Foundation for Basic Research, Government of Krasnoyarsk Territory, Krasnoyarsk Regional Fund of Science to the research projects no. 18-42-243009 r_mol_a and no. 19-43-240003 r_a, and the Foundation for Assistance to Small Innovative Enterprises in Science and Technology, contract no. 11843GU/2017, code 0033636, U.M.N.I.K. competition.

REFERENCES

1. C.-W. Nan, MRS Bull. **40**, 719 (2015). https://doi.org/10.1557/mrs.2015.196
2. O. A. Fouad, S. A. Makhlouf, G. A. M. Ali, and A. Y. El-Sayed, Mater. Chem. Phys. **128**, 70 (2011). https://doi.org/10.1016/j.matchemphys.2011.02.072
3. A. K. Rathore, S. P. Pati, M. Ghosh, et al., J. Mater. Sci.: Mater. Electron. **28**, 6950 (2017). https://doi.org/10.1007/s10854-017-6395-7
4. J. Xu, H. Yang, W. Fu, et al., J. Alloys Compd. **458**, 119 (2008). https://doi.org/10.1016/j.jallcom.2007.03.149
5. G.-R. Xu, J.-J. Shi, W.-H. Dong, et al., J. Alloys Compd. **630**, 266 (2015). https://doi.org/10.1016/j.jallcom.2015.01.067
6. E. B. Dokukin, R. V. Erhan, A. Kh. Islamov, et al., Phys. Status Solidi B **250**, 1656 (2013). https://doi.org/10.1002/pssb.201248379
7. R. Goyal, S. Lamba, and S. Annapoorni, Phys. Status Solidi A **213**, 1309 (2016). https://doi.org/10.1002/pssa.201532704

8. S. P. Pati, B. Bhushan, and D. Das, J. Solid State Chem. **183**, 2903 (2010). https://doi.org/10.1016/j.jssc.2010.09.037
9. N. R. Panda, S. P. Pati, A. Das, and D. Das, Appl. Surf. Sci. **449**, 654 (2018). https://doi.org/10.1016/j.apsusc.2017.12.003
10. B. Gokul, P. Saravanan, V. T. P. Vinod, et al., Powder Technol. **274**, 98 (2015). https://doi.org/10.1016/j.powtec.2015.01.002
11. Y. Cao, N. Kobayashi, Y.-W. Zhang, et al., J. Appl. Phys. **122**, 133903 (2017). https://doi.org/10.1063/1.5005620
12. V. G. Myagkov, I. A. Tambasov, O. A. Bayukov, et al., J. Alloys Compd. **612**, 189 (2014). https://doi.org/10.1016/j.jallcom.2014.05.176
13. L. E. Bykova, V. S. Zhigalov, V. G. Myagkov, et al., Phys. Solid State **60**, 2028 (2018). https://doi.org/10.21883/FTT.2018.10.46535.087
14. V. G. Myagkov, L. E. Bykova, V. S. Zhigalov, et al., J. Alloys Compd. **724**, 820 (2017). https://doi.org/10.1016/j.jallcom.2017.07.081
15. M. N. Volochaev, S. V. Komogortsev, V. G. Myagkov, et al., Phys. Solid State **60**, 1409 (2018). https://doi.org/10.21883/FTT.2018.07.46132.025
16. V. G. Myagkov, L. E. Bykova, O. A. Bayukov, et al., J. Alloys Compd. **636**, 223 (2015). https://doi.org/10.1016/j.jallcom.2015.02.012
17. V. G. Myagkov, V. S. Zhigalov, L. E. Bykova, et al., J. Alloys Compd. **665**, 197 (2016). https://doi.org/10.1016/j.jallcom.2015.12.257
18. Z. G. Qiu, D. C. Zeng, L. Z. Zhao, et al., Phys. B (Amsterdam, Neth.) **500**, 111 (2016). https://doi.org/10.1016/j.physb.2016.07.029
19. J. J. Lin, Z. Y. Pan, S. Karamat, et al., J. Phys. D: Appl. Phys. **41**, 095001 (2008). https://doi.org/10.1088/0022-3727/41/9/095001
20. T. Shiroyama. B. S. D. Ch. S. Varaprasad, Y. K. Takahashi, and K. Hono, AIP Adv. **6**, 105105 (2016). https://doi.org/10.1063/1.4964930
21. W. B. Cui, B. Varaprasad, Y. K. Takahashi, et al., Solid State Commun. **182**, 17 (2014). https://doi.org/10.1016/j.ssc.2013.11.010
22. Y. Yu, J. Shi, and Y. Nakamura, J. Appl. Phys. **109**, 07C1031 (2011). https://doi.org/10.1063/1.3536789
23. R. Tang, W. Zhang, and Y. Li, J. Magn. Magn. Mater. **322**, 3490 (2010). https://doi.org/10.1016/j.jmmm.2010.06.051
24. R. Tang, W. Zhang, and Y. Li, J. Alloys Compd. **496**, 380 (2010). https://doi.org/10.1016/j.jallcom.2010.02.018
25. C. W. White, S. P. Withrow, J. D. Budai, et al., J. Appl. Phys. **98**, 114311 (2005). https://doi.org/10.1063/1.2138801
26. V. G. Myagkov, V. S. Zhigalov, L. E. Bykova, et al., JETP Lett. **102**, 393 (2015). https://doi.org/10.7868/S0370274X15180071
27. V. G. Myagkov, L. E. Bykova, V. S. Zhigalov, et al., J. Alloys Compd. **706**, 447 (2017). https://doi.org/10.1016/j.jallcom.2017.02.261
28. V. G. Myagkov, V. S. Zhigalov, L. E. Bykova, et al., Phys. Status Solidi B **249**, 1541 (2012). https://doi.org/10.1002/pssb.201248064
29. V. G. Myagkov, L. E. Bykova, V. Yu. Yakovchuk, et al., JETP Lett. **105**, 610 (2017). https://doi.org/10.7868/S0370274X1710006X

Translated by E. Bondareva